



RESEARCH LETTER

10.1002/2016GL068323

Key Points:

- Seasonally varying eddy-mean flow interaction controls recirculation of Atlantic Water in Fram Strait
- The bulk recirculation occurs in a cyclonic gyre around the Molloy Hole at 80 degrees north
- A colder westward current south of 79 degrees north relates to the Greenland Sea Gyre, not removing Atlantic Water from the slope current

Supporting Information:

- Supporting Information S1
- Movie S1

Correspondence to:

T. Hattermann,
tore.hattermann@akvaplan.niva.no

Citation:

Hattermann, T., P. E. Isachsen, W.-J. von Appen, J. Albrechtsen, and A. Sundfjord (2016), Eddy-driven recirculation of Atlantic Water in Fram Strait, *Geophys. Res. Lett.*, 43, doi:10.1002/2016GL068323.

Received 17 FEB 2016

Accepted 21 MAR 2016

Accepted article online 24 MAR 2016

©2016. The Authors.

This is an open access article under the terms of the Creative Commons Attribution-NonCommercial-NoDerivs License, which permits use and distribution in any medium, provided the original work is properly cited, the use is non-commercial and no modifications or adaptations are made.

Eddy-driven recirculation of Atlantic Water in Fram Strait

Tore Hattermann^{1,2}, Pål Erik Isachsen^{3,4}, Wilken-Jon von Appen², Jon Albrechtsen⁵, and Arild Sundfjord⁶

¹Akvaplan-niva AS, High North Research Centre, Tromsø, Norway, ²Alfred Wegener Institute, Helmholtz Centre for Polar and Marine Research, Bremerhaven, Germany, ³Norwegian Meteorological Institute, Oslo, Norway, ⁴Institute of Geosciences, University of Oslo, Oslo, Norway, ⁵Institute for Marine Research, Bergen, Norway, ⁶Norwegian Polar Institute, Tromsø, Norway

Abstract Eddy-resolving regional ocean model results in conjunction with synthetic float trajectories and observations provide new insights into the recirculation of the Atlantic Water (AW) in Fram Strait that significantly impacts the redistribution of oceanic heat between the Nordic Seas and the Arctic Ocean. The simulations confirm the existence of a cyclonic gyre around the Molloy Hole near 80°N, suggesting that most of the AW within the West Spitsbergen Current recirculates there, while colder AW recirculates in a westward mean flow south of 79°N that primarily relates to the eastern rim of the Greenland Sea Gyre. The fraction of waters recirculating in the northern branch roughly doubles during winter, coinciding with a seasonal increase of eddy activity along the Yermak Plateau slope that also facilitates subduction of AW beneath the ice edge in this area.

1. Introduction

The Fram Strait (Figure 1a) is a major gateway for exchanges between the Atlantic and Arctic Oceans. Warm and salty Atlantic Water (AW), originating from the Gulf Stream/North Atlantic Current, flows northward along the eastern rim of the Nordic Seas toward the Fram Strait where it meets colder and fresher water masses of Arctic origin. The AW in the West Spitsbergen Current (WSC) has warmed since the 1990s [Beszczynska-Möller *et al.*, 2012], and the increased heat transport may contribute to the reduction of sea ice in the Arctic [Polyakov *et al.*, 2010; Rippeth *et al.*, 2015]. Inflow of AW also supplies nutrients for the Arctic Ocean ecosystem [Torres-Valdés *et al.*, 2013].

But not all of the AW reaching Fram Strait enters the Arctic Ocean proper. Marnela *et al.* [2013] estimated that about half of the AW transported in the WSC recirculates between 76 and 81°N. This portion becomes part of the southward flowing East Greenland Current (EGC). Together with modified AW that has looped around the Arctic Ocean, as well as with cold and fresh Polar Water (PW) and Arctic Ocean Deep Water (AODW), it ultimately contributes to the planetary-scale Meridional Overturning Circulation [Mauritzen, 1996; Rudels *et al.*, 2002; Våge *et al.*, 2013]. In the recent Coordinated Ocean-ice Reference Experiments [Iliack *et al.*, 2016] the “short cut” of AW recirculation in the Fram Strait was identified as a major source of uncertainty and model spread, and it is evident that a better understanding of the recirculation dynamics in Fram Strait is necessary to assess the heat budget of the Arctic Ocean as well as the fate of AW at high northern latitudes.

After early evidences of recirculation in Fram Strait [Perkin and Lewis, 1984; Manley, 1995], a mooring array crossing the strait along 78°50'N, which has been maintained since 1997 by the Norwegian Polar Institute and the Alfred Wegener Institute [de Steur *et al.*, 2009; Beszczynska-Möller *et al.*, 2012], is clearly showing westward flow—recirculation—in the central part of the strait. In addition to this “southern” recirculation branch, hydrographic observations and drifter data from the Marginal Ice Zone Experiment [Johannessen *et al.*, 1987] have indicated recirculation at about 80°N that appears to be associated with a cyclonic gyre around the Molloy Hole (marked MH in Figure 1a) [Quadfasel *et al.*, 1987]. Further observational evidence of this “northern” branch is, however, limited, and a conceptual lowest-order model of the recirculation there is lacking.

It is known that currents have a strong barotropic component in this weakly stratified high-latitude region and thus approximately follow the bottom topography or, more precisely, f/H contours, where f is the Coriolis parameter and H the water depth [Isachsen *et al.*, 2003; Nøst and Isachsen, 2003]. Thus, any theory must consider the complex bottom topography and f/H field in the Fram Strait (Figure 1a). Winds account for temporal variability of surface drift [Tsukernik *et al.*, 2010; Halvorsen *et al.*, 2015], and de Steur *et al.* [2014] have argued that the seasonality in the southern recirculation is part of the large-scale wind-driven cyclonic circulation of the Nordic Seas. Mesoscale eddies are thought to be important by removing AW from the WSC

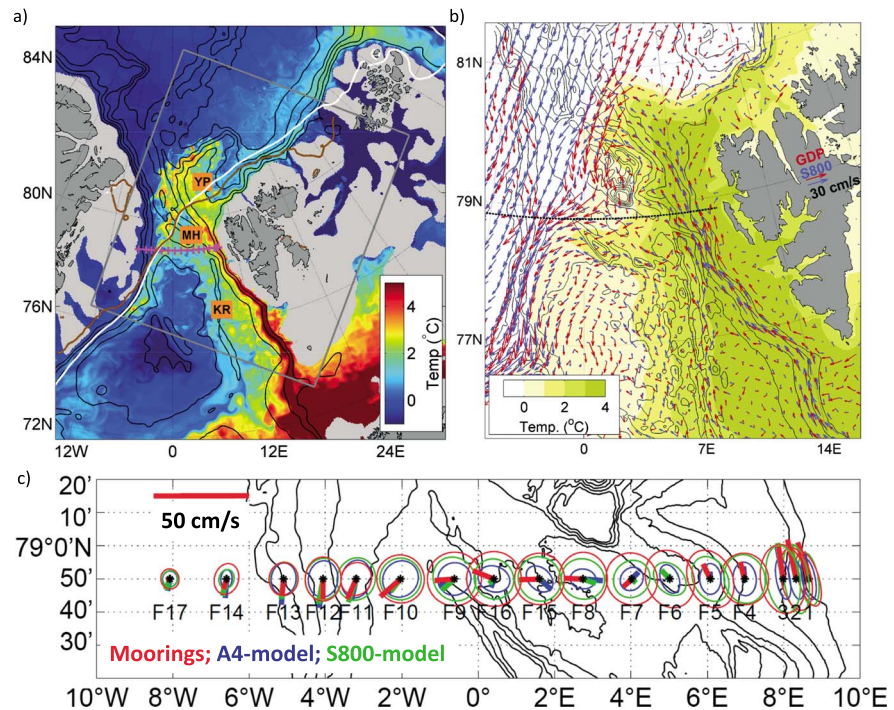


Figure 1. (a) Map of bathymetry in Fram Strait (black contours) together with A4-model and S800-model composite daily mean (15 March 2009) temperature at 250 m depth and contours of modeled (A4-model, white) and observed [Spreen *et al.*, 2008] (brown) multiyear averaged 75% sea ice extent. The grey box indicates the S800-model domain, FS mooring array positions are shown in magenta, and letters denote the Knipovich Ridge (KR), Molloy Hole (MH), and Yermak Plateau (YP). (b) Mean surface velocities from GDP data set (orange) together with mean surface velocity (blue) and mean surface temperature from the S800-model. (c) Mean currents and variance ellipses from the 75 m FS mooring array and corresponding model results that were saved with hourly frequency at these locations.

[Schauer *et al.*, 2004; Teigen *et al.*, 2011; Walczowski, 2013], and von Appen *et al.* [2016] show that the increase of eddy kinetic energy (EKE) in winter can readily be explained by enhanced baroclinic instability during this season.

In numerical models, the AW recirculation in the Fram Strait is generally seen as a bifurcation of the offshore branch of the WSC along the Knipovich Ridge (KR in Figure 1) [Aksenov *et al.*, 2010]. But Fieg *et al.* [2010] also report that AW pathways changed significantly when their model resolution was increased from $1/4^\circ$ to $1/12^\circ$ (about 27 km and 9 km). Only their higher-resolution simulation resolved the northern recirculation branch, with qualitative differences between the two models appearing to be related to the emergence of mesoscale eddies. A recent study by Kawasaki and Hasumi [2016], achieving model resolution of 2–3 km, reveals an intense mesoscale eddy field in the entire Fram Strait. However, with an internal Rossby radius typically ranging between 3–6 km in the WSC [von Appen *et al.*, 2016] and ~ 6 km in the EGC [Zhao *et al.*, 2014], the models discussed above should be considered eddy permitting rather than fully eddy resolving, with a clear picture of how eddy dynamics affect the AW transport in Fram Strait still largely missing.

To look further into how eddies transport AW around and also interact with the mean flow, this study presents results from a new high-resolution coupled sea ice-ocean model of the Fram Strait and Svalbard region (grey box in Figure 1a). With a horizontal grid spacing of 800 m, the simulations resolve bathymetric features and mesoscale dynamics with unprecedented detail. Trajectories of synthetic Lagrangian floats and Reynold fluxes were calculated to identify the spatial and temporal structure of AW pathways, and the conclusions are supported by comparing model results with statistical properties obtained from available observations.

2. Model Setup, Methods, and Data

2.1. The Arctic 4km and Svalbard 800m Model

Boundary conditions for the high-resolution Svalbard 800m model (S800-model) are provided by a coarser, 4 km pan-Arctic setup (A4-model). Both models are based on the Regional Ocean Modeling System

[Shchepetkin and McWilliams, 2005] and a coupled sea ice component [Budgell, 2005]. Bathymetry is based on the ETOPO1 topography, smoothed to achieve a commonly accepted maximum slope parameter [Haidvogel and Beckmann, 1999] of $s = |\Delta H|/2H \leq 0.35$. Vertically, both models are discretized into 35 levels with layer thickness of less than 1 m near the surface over the continental shelf and more than 100 m in the interior abyssal ocean.

The initial ocean state and lateral boundary conditions of the A4-model are provided by monthly averaged global reanalyses [Storkey *et al.*, 2010]. The S800-model is initialized and forced with daily averages from the A4-model. Tidal forcing is added along the open boundaries from the global TPXO tidal model [Egbert and Erofeeva, 2002]. Surface atmospheric forcing is provided by ERA-Interim reanalysis [Dee *et al.*, 2011] and climatological river input from all major rivers in the area [Martinsen *et al.*, 1992]. The S800-model also includes freshwater runoff from the Svalbard archipelago, estimated from glaciological mass balance provided by J. Kohler and C. Nuth, NPI and UiO (personal communication, 2014).

The A4-model was initialized with an ice-free ocean in summer 1993 and then spun-up for a 10 year period. The S800-model was initialized from January 2005, and the analysis shown in this study is based on model fields from July 2005 to July 2010. This represents a multiyear average that allows for comparison with modern in situ and remote sensing observations from the region.

2.2. Lagrangian Floats Simulations and Trajectory Statistics

Trajectories of neutrally buoyant floats were computed with TRACMASS [Döös, 1995] using 3-D daily averaged model velocities, which remove high-frequency variability such as tides but resolve the mesoscale eddy field. Approximately 78,000 floats were released every 10 days throughout the simulated period. The floats were evenly spaced between the surface and 1000 m depth over a cross section along the southwestern boundary of the S800-model domain, approximately between 0E and 15E. Each trajectory was tracked for 180 days, during which daily floats positions and corresponding temperature and salinity values were stored.

The trajectories were divided into three different “pathway groups” [von Appen *et al.*, 2014] based on the sections shown in red in Figure 2a. Trajectories crossing P2 but never crossing P1 or P3 were denoted the southern recirculation (SR), trajectories crossing P1 and P2 were denoted the northern recirculation (NR), and trajectories crossing P1 and P3 were denoted the Arctic Ocean inflow (AO). The daily floats positions within each group were binned on a $4\text{ km} \times 4\text{ km}$ horizontal grid, and the typical circulation pattern was assessed by computing the relative trajectory density distribution $D(x, y) = n_{x,y}/n_{\text{group}}$, where $n_{x,y}$ is the number of floats that visited a given bin at least once during the simulation and n_{group} is the total number of trajectories within the respective group.

For each pathway group, the potential temperature-salinity (T - S) distribution $\delta(T, S) = n_{T,S}$ was computed as the frequency of occurrence of individual T - S pairs, evaluated for all trajectories within the group at the floats position closest to the point denoted in Figure 2a, with S for the southern and N for the two northern pathways, and binned onto a regular grid of 0.25°C and 0.025 . For each group, a typical T - S ensemble was defined as all bins with $\delta(T, S) > \sqrt{\delta_{\text{max}}}$, where δ_{max} is the maximum count in any bin of the respective group.

Not all floats that passed P1 did eventually also pass either P2 or P3 during the tracking period. Some remain stagnant over the Yermak Plateau, while a few leave the area without passing through another section. For the figures presented here, only floats that started 120 days or less before passing P1 were counted (about 348,000 during the 5 year simulation), yielding a residual fraction of about 18% that was stagnant or wandered off. The average travel time was about 24 days from P1 to P2 (recirculation) and about 21 days from P1 to P3 (Arctic Ocean inflow), while 40 days after passing P1 about 75% of all accounted floats had either passed P2 or P3. Note that the Arctic Ocean inflow pathway also includes the trajectories around the northern rim of the Yermak Plateau, contributing with about 2% to that group for the chosen tracking period.

2.3. Supporting Observations

Three different multiyear observational data sets frame the model analysis. Their specific time periods vary, but since our focus is on seasonal and shorter (mesoscale) time scales, we use the longest possible data sets in order to increase the statistical reliability of comparisons.

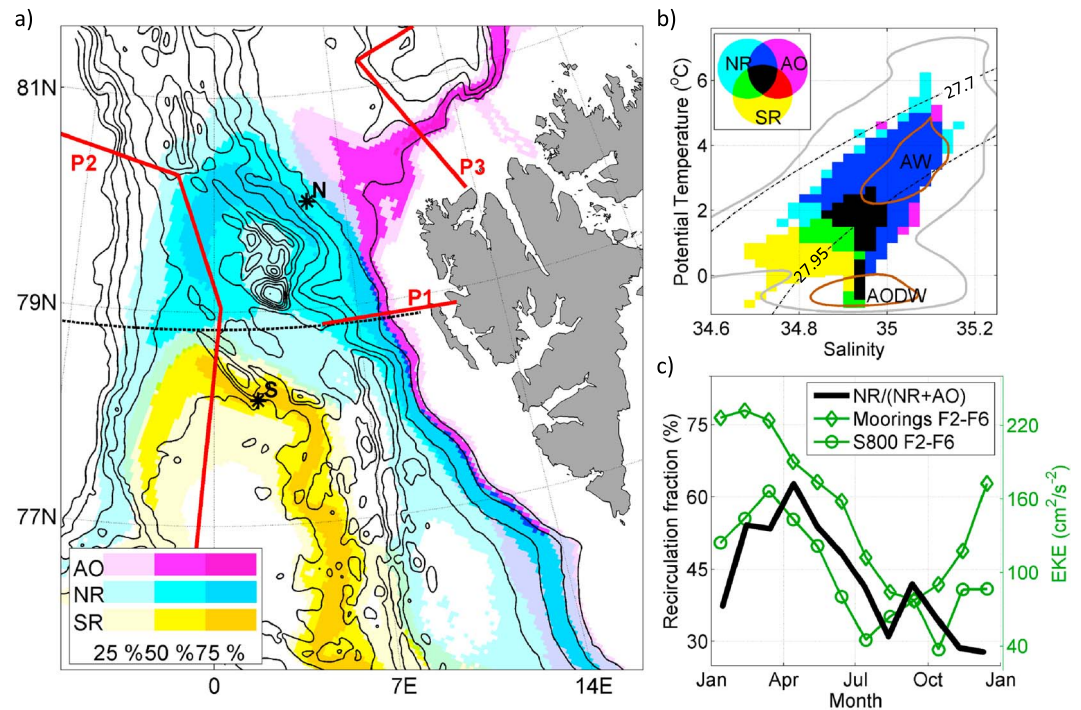


Figure 2. (a) A map of the relative trajectory density distribution of the southern recirculation (SR), northern recirculation (NR), and Arctic Ocean inflow (AO) pathway groups, being defined by the sections P1–P3 and shown as the percentage of all floats within each group. (b) T - S ensembles of each pathway group with most frequently (brown, 95% percentile) and commonly observed (grey, 50% percentile) T - S ensembles at the FS mooring array, with contours being smoothed for simplicity. (c) Time series of monthly averaged recirculation fraction ($NR/(NR + AO)$) together with observed and simulated EKE at the WSC mooring locations F2–F6. The recirculation fraction shown in January accounts for all floats that were passing P1 between 1 and 31 January and so forth for the other months. Monthly values of EKE from multiple years and moorings are averaged for all Januaries, all Februaries, etc.

Velocity and water mass statistics were obtained from 17 moorings across Fram Strait at 78°50'N, with nomenclature and locations shown in Figure 1c and referred to as the “FS mooring array” hereafter. Details on instrumentation and treatment of the data, which are available in PANGAEA [Beszczynska-Möller et al., 2015], are given in von Appen et al. [2016]. Being originally located at 79°N, in 2002 the westernmost moorings (F9–F14) were moved south to line up with the rest of the array and here we only consider the records at 78°50'N. Based on bihourly and hourly current meter time series at 75 m depth from 1997 (or 2002) to 2012, mean velocity vectors, associated variance ellipses, and monthly averages of eddy kinetic energy ($EKE = \frac{1}{2}[(u'u') + (v'v')]$, decomposing the velocity $\mathbf{u} = \bar{\mathbf{u}} + \mathbf{u}'$ into a monthly mean and daily averaged fluctuating component) were computed. Using the same algorithm as for the trajectory data, an observed T - S distribution was computed from hourly time series from all moorings at 75 m and 250 m depth. Ensembles of the most frequently observed T - S members were defined as the 95% and 50% percentiles of the resulting histogram after sorting all bins according to their frequency of occurrence.

A map of surface currents was obtained from 6-hourly displacements from 113 surface drifters that passed through Fram Strait between 1991 and 2014 as part of the global drifter program [Lumpkin et al., 2013] and are referred to as the GDP data set hereafter. Eulerian velocities were computed on a 64×64 grid covering 75°N, 15°E to 82°N, 20°W with the polysmooth function of Lilly [2015], which fits a least squares parabolic surface by weighting data in the vicinity of each grid point with an Epanechnikov kernel that includes up to 90 data points within a maximum cutoff radius of 50 km. Note that the GDP data provide information only about horizontal surface currents and are thus not suitable for the type of pathway group analysis that was carried out for the synthetic floats (which were advected by the 3-D velocity field).

Sea ice concentration fields were obtained from the Advanced Microwave Scanning Radiometer sensors AMSR-E and AMSR-2 for the years 2004–2013 [Spreen et al., 2008], and the position of the sea ice edge was identified as the contour limiting the area with ice concentration exceeding 75%.

3. Results

3.1. General Circulation Patterns and Comparison With Observations

The instantaneous temperature field at 250 m depth (Figure 1a) illustrates the AW distribution in the Fram Strait region in the S800-model. In addition to the warm core of the WSC along the Svalbard continental slope, an abundance of circular features and filaments indicates the presence of coherent vortices and eddy-induced advection in the central Fram Strait and over the slopes of the Yermak Plateau. Animations of the circulation (Movie S1 in the supporting information) show that some of the warm-core eddies that are constantly shed from the WSC are advected across the Fram Strait all the way to the EGC. It can also be seen that warmer subsurface water extends far beyond the ice edge, indicating the presence of horizontal and vertical frontal structures that will be discussed in greater detail later.

Figure 1b shows the time-mean simulated surface temperatures and currents, where currents can be compared to drifter velocities in the GDP data set. Being drogued at 15 m depth, the drifters generally track near-surface currents, although some might be caught by the sea ice, as suggested by the discrepancy between observations and model results in the northern parts of the domain. But generally, and despite the sparsity of the observational data set, the model velocities correspond strikingly to the drifter velocities. In particular, both vector fields show two distinct regions of westward flow in the central Fram Strait: a southern region at about 78.5°N where currents roughly trace out the large-scale topography of the Greenland Sea and a northern region west of the Yermak Plateau at 80°N where currents turn west along the northern flank of the Molloy Hole. Both regions are associated with tongues of higher mean surface temperatures that trace out southern and northern AW recirculation pathways.

The time-mean current vectors along the FS mooring array (Figure 1c) show that the simulations reproduce the observed flow speeds and directions of the boundary currents (F1–F5 and F10–F17), suggesting a realistic representation of overall mean transports at both model resolutions. Discrepancies exist in the central Fram Strait, at moorings F7, F8, F15, and F16, where neither model reproduces the observed mean westward flow. However, closer examination reveals that the currents in this region are sensitive to small displacements of the mean currents over rugged topography, and a few kilometers south of the actual mooring positions the S800-model indeed shows a westward mean flow. This delicate positioning of the central moorings at the northern rim of a westward flow regime is also consistent with the increased southward transport of the EGC after the relocation of the western moorings, as discussed by *de Steur et al.* [2014].

The size and orientation of the variance ellipses from the simulated currents also agree with the observations but with larger differences between the two model resolutions. In the central Fram Strait at F6–F9, where observed fluctuations generally exceed the mean flow (large, circular variance ellipses), the A4-model significantly underestimates the current variability, indicating that relevant mesoscale dynamics are not resolved at those scales.

Both models reproduce the distribution of different water masses in the Fram Strait region seen in the monthly and annual mean hydrography from the NOAA Arctic Ocean climatology [*Seidov et al.*, 2015] (not shown). A direct comparison of the model results with summer CTD sections and mooring time series also shows realistic water masses and isopycnal slopes (shown, e.g., in *von Appen et al.*, 2016, Figure 3), although with a general cold bias of up to 1°C in the AW during summer and slightly less during winter in both models, presumably being introduced in the A4-model upstream of the study area.

3.2. Recirculation Pathways From Lagrangian Floats

The relative trajectory density distributions of the three different pathway groups (Figure 2a) show that waters recirculating south and north of the FS mooring array have completely different origins. The majority of floats recirculating south of 79°N (yellow shading) originate from nondivergent trajectories along the western flanks of the Knipovich Ridge system, tracing out the large-scale ambient f/H contours of the Greenland Sea Gyre that skirts the FS mooring array. A few floats originate from the northward extension of the Norwegian Atlantic Front Current farther east, but these must have been advected by transients since the time-mean currents in Figure 1b show no persistent flow across the ridge system. In contrast, the northern recirculation (blue shading) exclusively consists of floats originating from east of the Knipovich Ridge where trajectories south of the FS mooring array are focused along the steep parts of the Svalbard continental slope.

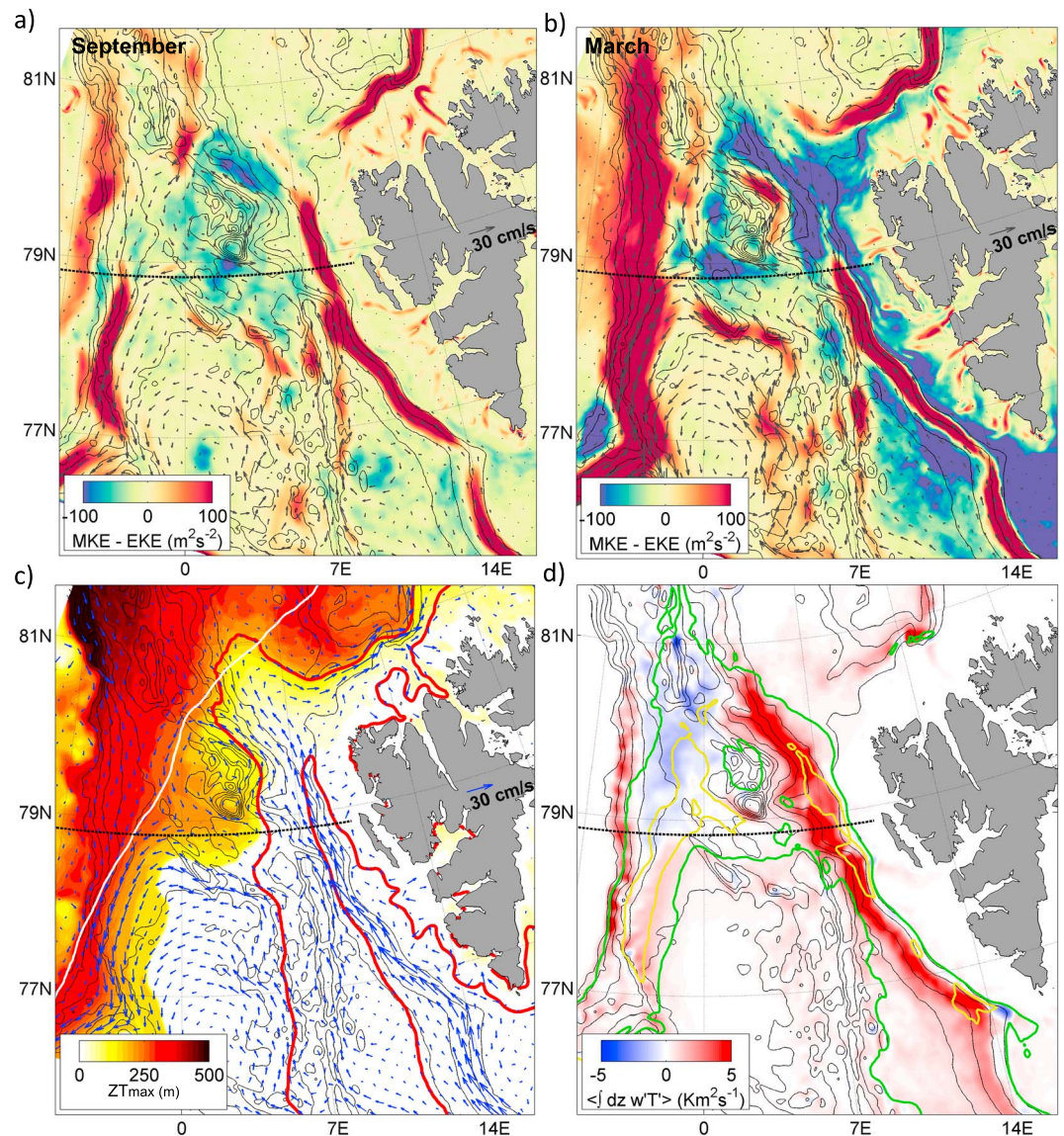


Figure 3. S800-model monthly mean differences between mean and eddy kinetic energy (MKE-EKE) at 75 m depth for (a) September and (b) March together with mean velocities. (c) 2005–2010 mean depth of the temperature maximum (z_{Tmax}) together with mean currents at this depth. White contour indicates the S800-model 75% mean sea ice extent, while red contours indicate the 2°C and 4°C isotherm at z_{Tmax} . (d) Depth-integrated, 5 year mean vertical eddy temperature fluxes with negative values (blue) denoting downward fluxes. Contours delineate areas where vertically integrated EKE exceeds $25 \times 10^5 \text{ m}^3 \text{ s}^{-2}$ (green) and $50 \times 10^5 \text{ m}^3 \text{ s}^{-2}$ (yellow).

Where the slope widens at the southwestern rim of the Yermak Plateau, the trajectories become more dispersive and divergent, either entering the Arctic Ocean (magenta shading) or turning west to recirculate in a coalescent flow along the northern flank of the Molloy Hole.

The T - S ensembles in Figure 2b show distinct water masses associated with the two recirculation pathways. The warmest and most saline signature of AW is seen in the Arctic Ocean inflow and in the northern recirculation. In contrast, water masses in the southern recirculation are colder and fresher, resembling the mixing line between AW and the cold and saline AODW in Figure 2b. This is consistent with the trajectory density distribution and suggests that water masses of the southern recirculation mainly originate from the Greenland Sea gyre and from the Norwegian Atlantic Front Current [Mork and Skagseth, 2010; Walczowski, 2013], in which AW has been significantly more cooled before reaching the Fram Strait than the water which reaches the northern recirculation within the much swifter WSC.

3.3. The Role of Eddies

3.3.1. Eddy-Induced Recirculation

The typical seasonal evolution of the northern “recirculation fraction” is shown in Figure 2c, here being defined as the number of floats passing both sections P1 and P2 divided by the number of all the floats passing P1 and either P2 or P3. The westward export of floats from the WSC is most efficient during late winter and spring, with a recirculation fraction of up to 60%, as opposed to 30% during summer. Figure 2c also shows that the recirculation fraction roughly resembles the observed and simulated EKE in the WSC, a field which increases during winter due to enhanced baroclinic instability of the boundary current (see *von Appen et al.* [2016] for a further analysis of the WSC stability properties).

To further illustrate the correspondence between the northern recirculation and EKE, Figures 3a and 3b show the difference between mean kinetic energy (MKE) and EKE for September and March. Mean advection dominates along the WSC in late summer, thus tending to transport AW along large-scale f/H contours—most of which turn east into the Arctic. In late winter, however, EKE dominates along the flanks of the entire WSC, particularly north of the FS mooring array where also the most dispersive float trajectories are seen. So eddy stirring in winter can be expected to divert AW off the main f/H contours and, hence, westward.

But also, the Molloy Hole gyre appears to be important for the northern recirculation. Animations of the circulation (Movie S1) show that anticyclonic vortices erode the WSC as it approaches the Yermak Plateau and relocate AW from the WSC to f/H contours that close around the Molloy Hole. The warm anticyclones are then efficiently advected westward by the Molloy gyre mean cyclonic circulation. Finally, eddy stirring west of the Molloy gyre transports AW onto geostrophic contours that guide the southward flowing EGC. Hence, it is a seasonally varying *advective-diffusive* interplay, where eddies “diffuse” AW between different sets of f/H contours [see, e.g., *Straneo et al.*, 2003], that seems to explain the net float transport pattern seen in Figure 2a.

3.3.2. Eddy-Induced Subduction

As AW recirculates in the Fram Strait it enters a zone of density compensation where the warm and salty AW has the same density as the cold and fresh PW. This frontal region is characterized by enhanced tidal mixing and water mass transformation [*Padman et al.*, 1992; *Fer et al.*, 2015]. In combination with air-sea-ice fluxes, this efficiently reduces the surface temperature along the northern recirculation pathway at 80°N, as can be seen from the temperature and velocity fields of Figure 1b and also in a plot of the depth $z_{T_{\max}}$ of the time-mean temperature maximum shown in Figure 3c. In the temperature-stratified eastern regions the warmest water resides at the surface, while in the density-compensated frontal zones between AW and PW the temperature maximum is found below. The temperatures on the $z_{T_{\max}}$ surface itself (not shown) also reveal an east-west gradient, indicating that water masses here are indeed irreversibly transformed.

Farther west along the recirculation pathway, however, salinity dominates the buoyancy, eventually forcing the westward flowing AW to subduct underneath the PW. While such vertical adjustment is difficult to obtain by the nearly nondivergent geostrophic flow, mesoscale eddies can efficiently mediate vertical temperature and buoyancy fluxes. The time-mean depth-integrated vertical eddy temperature flux in Figure 3d shows that eddy processes likely play an important role for this subduction of AW. Large upward eddy temperature fluxes along the WSC (red shading in Figure 3d), i.e., in the temperature-stratified east, imply a release of available potential energy as would be expected from baroclinic instability. Along the frontal zone itself, the vertical eddy fluxes are near zero, but in a large region west of the Molloy Hole they are distinctively negative (blue shading). This salt-stratified region is also associated with downward salt fluxes and therefore upward buoyancy fluxes (both not shown). So vertical eddy fluxes release available potential energy there too, and the subduction of AW underneath PW should be understood as a natural consequence of this ubiquitous tendency. Mesoscale dynamics, apparently, are therefore instrumental to both lateral and vertical advection of AW in the Fram Strait.

4. Conclusions

Eddy-resolving ocean simulations suggest a partial revision of the traditional picture of the AW pathways in the Fram Strait. Synthetic float trajectories show that the southern recirculation primarily relates to the Greenland Sea Gyre, while it causes little direct recirculation of AW transported by the WSC as earlier suggested by *Aksenov et al.* [2010]. Instead, the main recirculation route for the warmest AW is north of the Molloy Hole, where eddies interact with a time-mean cyclonic gyre that was first proposed by *Quadfasel et al.* [1987] and *Johannessen et al.* [1987]. The central part of the FS mooring array appears to be delicately located in a region of highly transient

flow, right at the boundary between the Greenland Sea and Molloy Hole gyres. These findings are consistent with the results of *de Steur et al.* [2014], who observed a stronger signal of the wind-driven large-scale flow along f/H contours in the Greenland Sea after a southward relocation of the westernmost parts of the FS mooring array.

Our estimate of the northern recirculation fraction roughly doubles in winter and spring, a seasonality that has not previously been described and appears to be directly tied to seasonally varying eddy activity. Enhanced storm activity in winter will project onto the EKE signal, but estimates of Eady growth rates [*von Appen et al.*, 2016] show that the WSC is more baroclinically unstable during winter months. In our model, the recirculation of the warm water relies on an advective-diffusive interplay between cross- f/H eddy diffusion and efficient westward mean flow advection along the northern rim of the Molloy Hole gyre—a process that will need more attention in the future. Eddies also appear to facilitate subduction of AW underneath PW west of the Molloy Hole, complementing buoyancy changes due to air-sea-ice fluxes and irreversible small-scale mixing [*Padman et al.*, 1992; *Sirevaag and Fer*, 2009] in determining the fate of AW in this region.

Acknowledgments

We thank Frank Gaarsted and three anonymous reviewers for their comments that significantly improved the manuscript. This study was supported by the Fram Centre project Arctic Ocean Flagship 6606-299, the NOTUR HPC project nn9238k and the Helmholtz Infrastructure Initiative FRAM.

References

- Aksenov, Y., S. Bacon, A. C. Coward, and A. J. G. Nurser (2010), The North Atlantic inflow to the Arctic Ocean: High-resolution model study, *J. Mar. Syst.*, *79*(1–2), 1–22.
- Beszczynska-Möller, A., E. Fahrbach, U. Schauer, and E. Hansen (2012), Variability in Atlantic water temperature and transport at the entrance to the Arctic Ocean, 1997–2010, *ICES J. Mar. Sci.*, *69*(5), 852–863.
- Beszczynska-Möller, A., W.-J. von Appen, and E. Fahrbach (2015), Physical oceanography and current meter data from moorings F1-F14 and F15/F16 in the Fram Strait, 1997–2012, *PANGAEA*, doi:10.1594/PANGAEA.150016.
- Budgell, W. P. (2005), Numerical simulation of ice-ocean variability in the Barents Sea region towards dynamical downscaling, *Ocean Dyn.*, *55*(3–4), 370–387.
- Dee, D. P., et al. (2011), The ERA-Interim reanalysis: Configuration and performance of the data assimilation system, *Q. J. R. Meteorol. Soc.*, *137*(656), 553–597.
- de Steur, L., E. Hansen, R. Gerdes, M. Karcher, E. Fahrbach, and J. Holfort (2009), Freshwater fluxes in the East Greenland Current: A decade of observations, *Geophys. Res. Lett.*, *36*, L23611, doi:10.1029/2009GL041278.
- de Steur, L., E. Hansen, C. Mauritzen, A. Beszczynska-Möller, and E. Fahrbach (2014), Impact of recirculation on the East Greenland Current in Fram Strait: Results from moored current meter measurements between 1997 and 2009, *Deep Sea Res., Part I*, *92*, 26–40.
- Döös, K. (1995), Inter-ocean exchange of water masses, *J. Geophys. Res.*, *100*, 13,499–13,514, doi:10.1029/95JC00337.
- Egbert, G. D., and S. Y. Erofeeva (2002), Efficient inverse modeling of barotropic ocean tides, *J. Atmos. Oceanic Technol.*, *19*(2), 183–204.
- Fer, I., M. Müller, and A. K. Peterson (2015), Tidal forcing, energetics, and mixing near the Yermak Plateau, *Ocean Sci.*, *11*(2), 287–304.
- Fieg, K., R. Gerdes, E. Fahrbach, A. Beszczynska-Möller, and U. Schauer (2010), Simulation of oceanic volume transports through Fram Strait 1995–2005, *Ocean Dyn.*, *60*(3), 491–502.
- Haidvogel, D. B., and A. Beckmann (1999), *Numerical Ocean Circulation Modeling*, Imp. College Press, London.
- Halvorsen, M. H., L. H. Smedsrud, R. Zhang, and K. Kloster (2015), Fram Strait spring ice export and September Arctic sea ice, *Cryosphere Discuss.*, *9*(4), 4205–4235.
- Iliack, M., et al. (2016), An assessment of the Arctic Ocean in a suite of interannual CORE-II simulations. Part III: Hydrography and fluxes, *Ocean Modell.*, *100*, 141–161, doi:10.1016/j.ocemod.2016.02.004.
- Isachsen, P. E., J. H. LaCasce, C. Mauritzen, and S. Hakkinen (2003), Wind-driven variability of the large-scale recirculating flow in the Nordic seas and Arctic Ocean, *J. Phys. Oceanogr.*, *33*(12), 2534–2550.
- Johannessen, J. A., et al. (1987), Mesoscale eddies in the Fram Strait marginal ice-zone during the 1983 and 1984 Marginal Ice Zone Experiments, *J. Geophys. Res.*, *92*, 6754–6772, doi:10.1029/JC092iC07p06754.
- Kawasaki, T., and H. Hasumi (2016), The inflow of Atlantic water at the Fram Strait and its interannual variability, *J. Geophys. Res. Oceans*, *121*, 502–519, doi:10.1002/2015JC011375.
- Lilly, J. M. (2015), jLab: A data analysis package for Matlab, v. 1.6. [Available at <http://www.jmlilly.net/jmlsoft.html>.]
- Lumpkin, R., S. A. Grodsky, L. Centurioni, M.-H. Rio, J. A. Carton, and D. Lee (2013), Removing spurious low-frequency variability in drifter velocities, *J. Atmos. Oceanic Technol.*, *30*(2), 353–360.
- Manley, T. O. (1995), Branching of Atlantic Water within the Greenland-Spitsbergen Passage: An estimate of recirculation, *J. Geophys. Res.*, *100*, 20,627–20,634, doi:10.1029/95JC01251.
- Marnela, M., B. Rudels, M. N. Houssais, A. Beszczynska-Möller, and P. B. Eriksson (2013), Recirculation in the Fram Strait and transports of water in and north of the Fram Strait derived from CTD data, *Ocean Sci.*, *9*(3), 499–519.
- Martinsen, E. A., H. Engedahl, G. Ottersen, B. Ådlandsvik, H. Loeng, and B. Balin (1992), MetOcean MModeling Project, Climatological and hydrographical data for hindcast of ocean currents, *Tech. Rep. 100*, 93 pp., The Norwegian Meteorol. Inst., Oslo, Norway.
- Mauritzen, C. (1996), Production of dense overflow waters feeding the North Atlantic across the Greenland-Scotland Ridge. Part 1: Evidence for a revised circulation scheme, *Deep Sea Res., Part I*, *43*(6), 769–806.
- Mork, K. A., and Ø. Skagseth (2010), A quantitative description of the Norwegian Atlantic Current by combining altimetry and hydrography, *Ocean Sci.*, *6*(4), 901–911.
- Nøst, O. A., and P. E. Isachsen (2003), The large-scale time-mean ocean circulation in the Nordic Seas and Arctic Ocean estimated from simplified dynamics, *J. Mar. Res.*, *61*(2), 175–210.
- Padman, L., A. J. Plueddemann, R. D. Muench, and R. Pinkel (1992), Diurnal tides near the Yermak Plateau, *J. Geophys. Res.*, *97*, 12,639–12,652, doi:10.1029/92JC01097.
- Perkin, R. G., and E. L. Lewis (1984), Mixing in the West Spitsbergen current, *J. Phys. Oceanogr.*, *14*(8), 1315–1325.
- Polyakov, I. V., et al. (2010), Arctic Ocean warming contributes to reduced polar ice cap, *J. Phys. Oceanogr.*, *40*(12), 2743–2756.
- Quadfasel, D., J. C. Gascard, and K. P. Koltermann (1987), Large-scale oceanography in Fram Strait during the 1984 Marginal Ice Zone Experiment, *J. Geophys. Res.*, *92*, 6719–6728, doi:10.1029/JC092iC07p06719.

- Rippeth, T. P., B. J. Lincoln, Y.-D. Lenn, J. A. M. Green, A. Sundfjord, and S. Bacon (2015), Tide-mediated warming of Arctic halocline by Atlantic heat fluxes over rough topography, *Nat. Geosci.*, *8*(3), 191–194.
- Rudels, B., E. Fahrbach, J. Meincke, G. Budéus, and P. Eriksson (2002), The East Greenland Current and its contribution to the Denmark Strait overflow, *ICES J. Mar. Sci. J. Cons.*, *59*(6), 1133–1154.
- Schauer, U., E. Fahrbach, S. Osterhus, and G. Rohardt (2004), Arctic warming through the Fram Strait: Oceanic heat transport from 3 years of measurements, *J. Geophys. Res.*, *109*, C06026, doi:10.1029/2003JC001823.
- Seidov, D., J. I. Antonov, K. M. Arzayus, O. K. Baranova, M. Biddle, T. P. Boyer, D. R. Johnson, A. V. Mishonov, C. Paver, and M. M. Zweng (2015), Oceanography north of 60 degrees N from World Ocean Database, *Prog. Oceanogr.*, *132*, 153–173.
- Shchepetkin, A. F., and J. C. McWilliams (2005), The regional oceanic modeling system (ROMS): A split-explicit, free-surface, topography-following-coordinate oceanic model, *Ocean Modell.*, *9*(4), 347–404.
- Sirevaag, A., and I. Fer (2009), Early spring oceanic heat fluxes and mixing observed from drift stations north of Svalbard, *J. Phys. Oceanogr.*, *39*(12), 3049–3069.
- Spreen, G., L. Kaleschke, and G. Heygster (2008), Sea ice remote sensing using AMSR-E 89-GHz channels, *J. Geophys. Res.*, *113*, C02503, doi:10.1029/2005JC003384.
- Storkey, D., E. W. Blockley, R. Furner, C. Guivarc'h, D. Lea, M. J. Martin, R. M. Barciela, A. Hines, P. Hyder, and J. R. Siddorn (2010), Forecasting the ocean state using NEMO: The new FOAM system, *J. Oper. Oceanogr.*, *3*(1), 3–15.
- Straneo, F., R. S. Pickart, and K. Lavender (2003), Spreading of Labrador sea water: An advective-diffusive study based on Lagrangian data, *Deep Sea Res., Part I*, *50*(6), 701–719.
- Teigen, S. H., F. Nilsen, R. Skogseth, B. Gjevik, and A. Beszczynska-Möller (2011), Baroclinic instability in the West Spitsbergen Current, *J. Geophys. Res.*, *116*, C07012, doi:10.1029/2011JC006974.
- Torres-Valdés, S., T. Tsubouchi, S. Bacon, A. C. Naveira-Garabato, R. Sanders, F. A. McLaughlin, B. Petrie, G. Kattner, K. Azetsu-Scott, and T. E. Whitledge (2013), Export of nutrients from the Arctic Ocean, *J. Geophys. Res. Oceans*, *118*, 1625–1644, doi:10.1002/jgrc.20063.
- Tsukernik, M., C. Deser, M. Alexander, and R. Tomas (2010), Atmospheric forcing of Fram Strait sea ice export: A closer look, *Clim. Dyn.*, *35*(7–8), 1349–1360.
- Våge, K., R. S. Pickart, M. A. Spall, G. W. K. Moore, H. Valdimarsson, D. J. Torres, S. Y. Erofeeva, and J. E. Ø. Nilsen (2013), Revised circulation scheme north of the Denmark Strait, *Deep Sea Res., Part I*, *79*, 20–39.
- von Appen, W.-J., I. M. Koszalka, R. S. Pickart, T. W. N. Haine, D. Mastropole, M. G. Magaldi, H. Valdimarsson, J. Girton, K. Jochumsen, and G. Krahnmann (2014), The East Greenland Spill Jet as an important component of the Atlantic Meridional Overturning Circulation, *Deep Sea Res., Part I*, *92*, 75–84.
- von Appen, W.-J., U. Schauer, T. Hattermann, and A. Beszczynska-Möller (2016), Seasonal cycle of mesoscale instability of the West Spitsbergen Current, *J. Phys. Oceanogr.*, doi:10.1175/JPO-D-15-0184.1, in press.
- Walczowski, W. (2013), Frontal structures in the West Spitsbergen Current margins, *Ocean Sci.*, *9*(6), 957–975.
- Zhao, M., M.-L. Timmermans, S. Cole, R. Krishfield, A. Proshutinsky, and J. Toole (2014), Characterizing the eddy field in the Arctic Ocean halocline, *J. Geophys. Res. Oceans*, *119*, 8800–8817, doi:10.1002/2014JC010488.